Crystal structure of the aminoglycosides N -acetyltransferase Eis2 from Mycobacterium abscessus

Kien Lam Ung, Husam M.A.B. Alsarraf, Vincent Oliéric, Laurent Kremer, Mickaël Blaise

PROF. LAURENT KREMER (Orcid ID : 0000-0002-6604-4458)

DR MICKAEL BLAISE (Orcid ID : 0000-0002-7860-3464)

Received Date : 19-Apr-2019

Revised Date : 22-May-2019

Accepted Date : 27-Jun-2019

Crystal structure of the aminoglycosides *N*-acetyltransferase Eis2 from *Mycobacterium abscessus*

Kien Lam Ung[1], Husam M.A.B. Alsarraf[1], Vincent Olieric[2], Laurent Kremer[1,3], and Mickaël Blaise*[1]

[1] Institut de Recherche en Infectiologie de Montpellier (IRIM), Université de Montpellier, CNRS UMR 9004, Montpellier, France.

[2] Swiss Light Source, Paul Scherrer Institute, CH-5232 Villigen, Switzerland.

[3] INSERM, IRIM, 34293 Montpellier, France.

***Corresponding author:**

Tel: (+33)0434359447; Email: mickael.blaise@irim.cnrs.fr

Institut de Recherche en Infectiologie de Montpellier (IRIM), Université de Montpellier, CNRS UMR 9004, Montpellier, France. www.irim.cnrs.fr

Running title: Structural and biochemical study of *M. abscessus* Eis2.

This document is the accepted manuscript version of the following article:

Ung, K. L., Alsarraf, H. M. A. B., Olieric, V., Kremer, L., & Blaise, M. (2019). Crystal structure of the aminoglycosides N-acetyltransferase Eis2 from Mycobacterium abscessus. FEBS Journal, 286(21), 4342-4355. https://doi.org/10.1111/febs.14975

Keywords: *Mycobacterium abscessus*, aminoglycosides, drug resistance mechanism, GCN5-related *N*-acetyltransferase, Eis2.

Abbreviations: Eis, Enhanced in intracellular survival; *Mabs, Mycobacterium abscessus*; *M.tb*, *Mycobacterium tuberculosis*, *M.smeg, Mycobacterium smegmatis;* KAN, kanamycin; HYG, hygromycin B; AMK, amikacin; SeMet, selenomethionine; ACO, acetyl-CoA; NTM, non-tuberculous mycobacterium; PDB, protein data bank; IPTG, Isopropyl-*β*-D-thiogalactoside; AG, aminoglycoside; PEG, polyethylene glycol;

Database: Structural data are available in the PDB database under the accession numbers : 6RFY , 6RFX and 6RFT.

Abstract

Mycobacterium abscessus is an emerging human pathogen that is notorious for being one of the most drug-resistant species of *Mycobacterium*. It has developed numerous strategies to overcome the antibiotic stress response, limiting treatment options and leading to frequent therapeutic failure. The panel of aminoglycosides usually used in the treatment of *M. abscessus* pulmonary infections is restricted by chemical modification of the drugs by the *N*-acetyltransferase Eis2 protein (*Mabs*_Eis2). This enzyme acetylates the primary amine of aminoglycosides, preventing these antibiotics from binding ribosomal RNA and thereby impairing their activity. In this study, the high-resolution crystal structures of *Mabs*_Eis2 in its *apo*- and cofactor-bound forms were solved. The structural analysis of *Mabs*_Eis2, supported by the kinetic characterization of the enzyme, highlights the large substrate specificity of the enzyme. Furthermore, *in silico* docking and biochemical approaches attest that *Mabs*_Eis2 modifies clinically relevant drugs such as kanamycin and amikacin, with a better efficacy for the latter. In line with previous biochemical and *in vivo* studies, our work suggests that *Mabs*_Eis2 represents an attractive pharmacological target to be further explored. The high-resolution crystal structures presented here may pave the way to the design of Eis2-specific inhibitors with the potential to counteract the intrinsic resistance levels of *M. abscessus* to an important class of clinically important antibiotics.

Introduction

Non-tuberculous mycobacterium (NTM) infections are on the rise and even surpassing tuberculosis in industrialized countries. Among them, the fast-growing species *Mycobacterium abscessus* is considered as an emerging human pathogen [1]. The *M. abscessus complex,* comprising three subspecies, *M. abscessus sensu stricto (Mabs)*, *M. abscessus subsp. bolletii* and *M. abscessus subsp. massiliense,* is responsible for a large set of clinical manifestations. These include cutaneous and soft tissues infections, disseminated infections as well as pulmonary diseases, particularly in patients with an underlying lung pathology (history of tuberculosis, bronchiectasis, neoplasia). However, in 30% of the cases, the subjects are free from any respiratory pathology, reflecting the virulent nature of this bacterium [2]. Patients with cystic fibrosis (CF) are particularly susceptible to NTM infections [3]. In addition, it was proposed that *Mabs* infections may not only be acquired solely by environmental strains but can also be transmitted between infected individuals, particularly among CF patients [4].

Standard chemotherapy against *Mabs* lung diseases involves aminoglycosides (amikacin), macrolides (clarithromycin) and *β*-lactams (cefoxitin and imipenem) [5]. However, one worrying aspect of the *M. abscessus complex* infections relies on the extreme resistance levels of these bacteria to most conventional antibiotics including all first-line anti-tubercular drugs (isoniazid, rifampicin, pyrazinamide) [6]. Mycobacterial species are naturally resistant to most classes of antibiotics due to the presence of a highly hydrophobic and impermeable cell wall [7] and the development of mechanisms allowing them to modify antibiotics, rendering them ineffective. For instance, RNA modifications such as methylation and mutation in target genes lead to resistance to aminoglycosides and macrolides [8],[9]. Other mechanisms involve the expression of a large set of efflux pumps, involving MmpL transporter family members, leading to resistance to thiacetazone derivatives, clofazimine and bedaquiline [10],[11],[12]. Another class of efflux pumps, comprising the major facilitator superfamily (MFS) transporter, has also been proposed recently to endorse a role in resistance to vancomycin, novobiocin, and rifampicin [13]. Antibiotic inactivation appears as another strategy employed by *Mabs* to overcome the effect of antibiotics [14], as exemplified by the production of a specific *β*-lactamase (Bla_{MAB}) degrading *β*-lactams, such as amoxicillin or imipenem, thereby considerably restricting the activity of these drugs and their use in clinical settings [15],[16]. Whereas streptomycin is inactivated by the 3"-*O*-phosphotransferase [APH(3")] encoded by *MAB_2385* [17], resistance to other aminoglycosides (AG) appears mediated by an *N*-acetyltransferase [18], which modifies AG by adding one or several acetyl groups, ultimately impairing their binding capacity to the ribosomes.

The *M. tuberculosis* (*M.tb*) *Eis* gene (Enhanced in Intracellular Survival) encodes an *N*-acetyltransferase belonging to the GCN5-related *N*-acetyltransferase (GNAT) that was originally discovered for its capacity to confer enhanced intra-macrophage survival when introduced in *M. smegmatis* [19]. *Eis* was also shown to modulate the immune response by controlling the secretion of IL-10 and TNF-α by monocytes in response to *M.tb* infection [20]. IL-10 induction modulates autophagy as a consequence of Eis-mediated histone acetylation [21]. The implication of Eis in autophagy modulation was also shown in another study along with its capacity to regulate inflammation and macrophage cell death [22]. That Eis *N*-acetylates Lysine residues, and notably the HU nucleoid protein, impeding its interaction with DNA and resulting in altering DNA compaction has been reported [23]. The enzyme modifies also the Lys55 residue of the dual phosphatase DUSP16/MKP-7, thus inhibiting the JNK-dependent autophagy, phagosome maturation, and generation of reactive oxygen species, therefore, aiding *M.tb* to survive within macrophages [24].

However, in addition to its important contribution in host-pathogen interactions, the activity of Eis in *N*-acetylating various AG is well documented. Up-regulation of Eis triggers resistance to kanamycin in *M.tb* clinical isolates [25]. Biochemical characterization of purified Eis from *M.tb* demonstrated its capability to acetylate a wide range of AG and its crystal structure was solved, revealing its belonging to the GCN5-related *N*-acetyltransferase family [26].

Eis-related proteins are also found in NTM [27], with *Mabs* possessing two Eis members, namely Eis1 (*Mabs*_Eis1) encoded by *MAB_4124* and Eis2 (*Mabs*_Eis2) encoded by the *MAB_4532c* gene. However, *Mabs*_Eis1 failed to show significant activity towards AG *in vitro* and a deletion of *Mabs_eis1* was not more associated with increased susceptibility to AG than the wild-type strain. In contrast, *Mabs*_Eis2 similarly to its *M.tb* homologue exhibits a broad specificity for AG substrates and can use acetyl-CoA as a cofactor and acetyl group donor. Consistently, a *Mabs_eis2* deletion mutant was more susceptible to AG, such as hygromycin B (HYG) and another antibiotic class notably capreomycin than the wild-type strain [28],[18]. In addition, this mutant showed also a reduced capacity of survival in macrophages as compared to its parental or complemented counterparts [29]. Expression of *Mabs_eis2* was shown to be up-regulated a 100 times upon exposure of *Mabs* culture to amikacin, *via* a mechanism implicating the master transcription regulator WhiB7, known to control the expression of many genes involved in drug resistance pathways [30].

Together, these studies strongly suggest that *Mabs*_Eis2 participates in AG resistance while *Mabs*_Eis1 is likely to exhibit another substrate specificity that remains to be discovered. That *Mabs*_Eis2 plays a dual role in AG resistance and persistence of the bacilli in macrophages makes it

an attractive target to be exploited in future pharmacological developments against *Mabs*. Since *Mabs*_Eis2 shares only moderate sequence identity with other Eis homologs, we attempted here to solve its crystal structure, aiming that it may help in guiding the design of specific inhibitors. In this study, we provide the biochemical characterization and the high-resolution crystal structures of *Mabs*_Eis2 in its *apo*-form and bound to acetyl-CoA.

Results and Discussion

*Mabs*_Eis2 purification and biochemical characterization

*Mabs*_Eis2 was expressed as a recombinant protein in *E. coli* and purified *via* a three-step purification procedure (Fig.1A). Although *Mabs*_Eis2 enzymatic activity has been previously investigated [28], we examined whether the protein purified under our conditions was active prior to engaging the subsequent structural studies. We determine the kinetic properties for acetyl-CoA (ACO) using kanamycin (KAN) (a mixture of kanamycin A (96%) and kanamycin B (4%)) as an acetyl group acceptor. Our results indicate that *Mabs*_Eis2 was active and displays the following kinetic parameters: K_M=36.2 ± 2.9 µM , k_{cat}=2.2 ± 0.12 s^{-1} , V_{max}=0.55 ± 0.03 µM.s^{-1} (Fig.1B). These values are in good agreement with kinetic constants of Eis proteins from other bacteria and notably of other mycobacterial species [31].

Crystal structure of the *Mabs*_Eis2 *apo*-form

Comforted by the biochemical data we engaged crystallization trials of *Mabs*_Eis2 as well as co-crystallization experiments in presence of ACO or HYG. Despite the possibility to obtain crystals for all the requested conditions mentioned above, we could not solve any co-crystal structure with AG. Alternative strategies relying on soaking experiments in the presence of a high concentration of either HYG or KAN also failed. However, we could solve two crystal structures of the *apo*-enzyme and the structure of ACO-bound *Mabs*_Eis2 complex.

All the x-ray structures of *Mabs*_Eis2 are belonging to the monoclinic space group $P2_1$ and share similar cell parameters (Table 1). The first *apo*-structure was obtained using the selenomethionine (SeMet)-derived protein and, was therefore, solved by the single-wavelength anomalous dispersion (SAD) method. These crystals were grown in presence of 0.2 M ammonium acetate, 0.1 M sodium citrate pH 5.6 and 30% polyethylene glycol (PEG) 4000 and 5 mM HYG. The structure was refined to 1.9 Å resolution. The asymmetric unit contains six molecules of which most

residues could be modeled with the exception of the three first residues in the N-terminus as well as the loops spanning from residues 234 to 239 in all chains and residues 119 to 124 in chains A, B, C. We could not observe any electron density corresponding to HYG but we could place without ambiguity six citrate, five acetate and seven PEG molecules.

The crystal of the native protein diffracting to 2.2 Å resolution (Table 1) was obtained in the following condition : 0.2 M Lithium sulfate monohydrate, 0.1 M BIS-TRIS pH 5.5 and 25% w/v PEG 3,350. The asymmetric unit contains also six macromolecules, most residues could be modeled with the exception of a few amino acids for each chain and as described: chain A (residues 2-233 and 239-411), chain B (residues 3-233, 238-411), chain C (residues 3-233, 237-411), chain D (residues 3-233, 236-411), chain E (residues 3-233, 239-411) and chain F (residues 4-233, 238-411). Five BIS-TRIS molecules and six sulfate ions could also be placed.

Analysis of the crystal packing with the PISA server [32] predicts the existence of a stable hexamer in the asymmetric unit. The multimeric nature of the protein was subsequently confirmed by size-exclusion chromatography (SEC), which indicated that *Mabs*_Eis2 behaves as a high-molecular-weight oligomer in solution, with an apparent calculated mass of 205 kDa, suggesting a tetramer or pentamer (M.W. theoretical of 45 kDa for the monomer) (Fig.1A). This discrepancy could be explained by the fact that the radius of gyration (*R*g) calculated with *Crysol* [33] of the trimer and hexamer exhibit very similar *R*g values, 39 and 42 Å (and therefore all intermediate forms have similar *R*g). Since the SEC elution profile is inherent to the globular shape of the macromolecule it is not unexpected that the apparent mass in solution is not in full adequation the expected hexameric form of the protein. So far, six structures of Eis proteins or "Eis-like proteins" from various microorganisms (*M.tb*, *Mycobacterium smegmatis*, *Anabaena variabilis, Enteroccus faecalis, Bacillus anthracis and Kribbella flavida*) have been deposited to the protein data bank. The crystals packing analysis of these structures confirm the hexameric form for all of them.

The *Mabs*_Eis2 overall structure is similar to one of its orthologs and is made of two trimers superposed on top of each other (Fig.2A). Each monomer is made of 16 beta-strands and 11 alpha-helices that can be divided into three domains: the N-terminal GNAT domain (residues 1-116), the central GNAT domain (residues 117-304) and the C-terminal domain (residues 305-411) (Fig.2B). Structural comparison attests that *Mabs*_Eis2 is similar to the Eis proteins from *Mycobacterium* species. Indeed, superposition of *Mabs*_Eis2 structure onto the *M.tb* protein (PDB : 3uy5, 28% primary sequence identity) [24] or onto the *M. smegmatis* one (PDB : 4qb9, 31% identity) [34], gives a similar r.m.s.d of 1.8 Å. This structural analysis indicates that *Mabs*_Eis2 is nonetheless more distant from the *M.tb* and *M. smegmatis* Eis proteins than they are from each other as they share

60% sequence identity and a low r.m.s.d (0.6 Å) when superposed on each other. *Mabs*_Eis2 diverges from the structures of Eis proteins of other bacterial genus since superposition of the structures with *Bacillus anthracis* protein (PDB id: 3n7z), *Enterococcus faecalis* (PDB id : 2hv2, unpublished), *Anabaena variabilis* (PDB id : 2ozg, unpublished) and *Kribbella flavida* (PDB id : 4my3, unpublished) generates respectively an r.m.s.d. of 2.1 Å over 350 residues (18% identity) [31], 2.3 Å over 356 residues (17% identity), 2.3 Å over 355 residues (18% identity), 2.7 Å over 350 residues (23% identity) (Fig.3 and Fig.4).

The structure analysis reveals also the presence of several ligands. The first *apo*-form binds to a molecule of BIS-TRIS occupying the AG-binding site while a sulfate ion is found at the same position than the phosphate group of ACO (Fig.5A and 5C). In the second *apo*-structure obtained with the SeMet-labeled protein, a citrate molecule occupies also the phosphate binding site of ACO while a PEG fragment is present in the AG-binding site (Fig.5B and 5D). However, none of these ligands seem to trigger structural rearrangements similar to those observed upon binding to ACO (Fig.5F) or to the movement of the loop made by residues 26-31 upon binding of AG in the *M.tb*:ACO:tobramycin structure (Fig.5E and 5F) or seen in the *M. smegmatis* Eis:paromomycin structure (not shown).

Co-crystal structure of *Mabs*_Eis2 bound to acetyl-CoA

The co-crystal structure of *Mabs*_Eis2 bound to ACO was solved by molecular replacement and refined to a resolution of 2.3 Å (Fig.6A), (Table 1). Most of the amino acids from the six monomers of the asymmetric unit could be placed with the exception of the first two or three Nt residues and the loop spanning from residues 232 to 239, which like in the *apo*-forms for any of the monomers, remains poorly defined. In all six subunits, a clear electron density is visible for ACO (Fig.6B). The cofactor could be rebuilt entirely in chains A, B and C while the acetyl and *β*-mercapto-ethylamine groups could not be placed in the other three chains.

The ACO binding site is defined by fourteen residues. Herein, we describe the interactions occurring with ACO in chain A (Fig.6C). The N and O groups from the main chain of Val85 provide a rather weak H-bond interaction with the N and P groups of ACO. The side chain of Arg91 makes H-bonding with the ACO ribose and adenine groups. The same residue contacts with its main chain the P group and creates also a salt-bridge between its side chain and the P group. Arg92, Gly94, Leu94, Leu95 interact *via* their main chain with the P groups of the 3',5' ADP by a complex H-bond network that is completed also with the side chain of Thr96. Glu120 interacts also with adenine group *via* H-bonds and Ser119 completes the H-bond interaction network. The main chain of Phe117 creates a

water-mediated H-bond with the acetyl group of ACO. Two hydrophobic interactions complete the interaction, notably by Val83 and Ile123. Arg126 interacts with the phosphate of the ribose by a salt-bridge and Asp226 from chain F interacts by H-bond through a water molecule with the ribose of ACO. Most of these residues are very well conserved in all Eis protein structures reported so far (Fig.4). With the exception of Phe117, all the amino acids contacting the cofactor are strictly conserved in other mycobacterial Eis proteins (Fig.4), further confirming the affiliation of *Mabs*_Eis2 to the mycobacterial clade.

The superposition of the ACO-bound structure onto the *apo*-form indicates that the two structures are very similar (r.m.s.d. of 0.54 Å) and that only a few structural rearrangements occur upon ACO binding (Fig.6D). Residues Ala121 to Phe127 that are part of the loop in the *apo*-form adopt an alpha-helical structure (α3') when ACO binds. Since these structures were obtained in the same crystal form, one can exclude that it is a packing artifact and, therefore, that ACO binding triggers this secondary structure reorganization. While this was not observed in the *M.tb* Eis structure, a similar structural change was reported in the *M. smegmatis* enzyme, whereby residues Gly124 to Gly130 that are part of a loop followed by a single helix-turn in the paromomycin-bound form (PDB id: 4qb9) adopt an alpha-helical conformation in the ACO-bound structure (PDB id : 3sxn) (Fig.6D) [34],[24]. The fact that this region folds always as an alpha-helix in all the other Eis structures either bound or not to ACO (not shown), suggests that this structural feature is maybe inherent to Eis proteins from the non-tuberculous mycobacterial origin.

Aminoglycosides recognition and catalytic efficiencies

As we could not solve any crystal structure of *Mabs*_Eis2 bound to AG we instead performed *in silico* docking of several antibiotics into the *Mabs*_Eis2:ACO structure. The docking box search was oriented thanks to the AG binding pockets previously identified in the *M.tb* [35] or *Msmeg* Eis [34] co-crystal structures. Docking poses allowing to position one of the primary amine group of HYG and KAN near the acetyl group of ACO could be obtained (Fig.7A and 7B). *Mabs*_Eis2 can also accommodate AMK in the binding pocket with binding energies similar to those determined for HYG and KAN (Fig.7B). This appears rather surprising based on previous work suggesting that AMK it is not a substrate of *Mabs*_Eis2 [28]. To confirm this prediction, kinetic assays were performed to compare the catalytic efficiencies of *Mabs*_Eis2 for the three antibiotics. All three AG were shown to be good substrates as they share similar catalytic efficiencies (k_{cat}/K_M), although the enzyme appears better at processing HYG and AMK rather than KAN since it presents about a ten times higher catalytic efficiency in the presence of HYG and AMK than KAN (Fig.7C and Table 2).

These docking poses allow us to propose the binding sites of all three AG and report the major residues interacting with the antibiotics that are contacted mainly by a complex H-bond network involving either the main chain or the side chains of the different amino acids. Tyr23, Arg28, Glu34, Thr81, and Ser194 appear as key residues as they interact with the three antibiotics. Asn38 and Phe117 by H-bonds and Phe26 interact only with AMK and HYG. Ser119, Leu197, Arg228, Gln245, and Asp410 are more specific to AMK, while Trp195, Ser199, Phe411 are only interacting with KAN. The residues involved in the binding of either paromomycin or tobramycin in the *M.tb* or *M.smeg* enzymes are not well conserved in *Mabs*_Eis2 (Fig.4 and Fig.7D).

In summary, we report here the high-resolution x-ray structure of *Mabs*_Eis2, previously shown to participate in resistance to AG resistance in *Mabs* [18],[30]. Of clinical importance, this work demonstrates that *Mabs*_Eis2 is involved in the direct modification of AMK, one of the most commonly used antibiotics for the treatment of *Mabs* infections [36]. Furthermore, we demonstrate the usefulness of the *in silico* docking strategy to assess the substrate specificity of *Mabs*_Eis2. This raises the attractive hypothesis of developing specific inhibitors of *Mabs*_Eis2 that would increase the susceptibility of *Mabs* to AG, paving the way to improved therapeutic options for *Mabs* infections. A similar strategy has recently been applied by using avibactam, a specific inhibitor of the beta-lactamase of *Mabs*, allowing to increase the susceptibility of *Mabs* to beta-lactam drugs [15],[16]. The crystal structures along with the *in silico* screening approach reported here may represent a starting point for searching such *Mabs*_Eis2 inhibitors.

Materials and methods

Expression and purification of *Mabs_E*is2

The optimized codon sequence of *Mabs_eis2* (*MAB_4532c)* was synthesized (Genscript) and cloned into pET-30a between the KpnI and EcoRI restriction sites with an additional Tobacco Etch Virus (TEV) protease cleavage site in frame with the N-terminal 6xHis and S-tags. *Escherichia coli* BL21 (DE3) strain resistant to Phage T1 (New England Biolabs) carrying the pRARE2 plasmid and transformed with pET-30a:*Mabs_eis2* was grown in six-liters flasks containing LB broth at 37^{o}C, under agitation at 180 rpm, and supplemented with 50 µg/mL KAN and 30 µg/mL chloramphenicol. When the OD_{600} reached ~0.8, cultures were chilled on ice for 30 min and induced with 1 mM of Isopropyl-*β*-D-thiogalactoside (IPTG) (Euromedex) for 16 h at 16^{o}C. Bacteria were pelleted by

centrifugation at 6,000 x *g* for 20 min and resuspended in buffer A (50 mM Tris-HCl pH 8, 0.4 M NaCl, 20 mM imidazole, 5 mM *β*-mercaptoethanol and 1 mM benzamidine). The cell lysate was obtained by sonication and subsequently clarified by centrifugation at 28,000 x *g*, at 4°C for 1 h. The resulting supernatant was loaded onto Ni-NTA sepharose resin by gravity and unbound proteins were discarded following washing with three column volumes with buffer A and buffer B (50 mM Tris-HCl pH 8, 1M NaCl and 5 mM *β*-mercaptoethanol). *Mabs*_Eis2 was eluted with buffer C (50 mM Tris-HCl pH8, 0.2 M NaCl, 5 mM β-mercaptoethanol and 250 mM imidazole). The eluate was incubated with TEV protease (1 mg of TEV protease per 40 mg of proteins) and dialyzed overnight against buffer D (20 mM Tris-HCl pH 7.4, 0.2 M NaCl and 5 mM *β*-mercaptoethanol). Uncleaved *Mabs*_Eis2 and the TEV His-tagged were removed by passing the dialyzed eluate through a Ni-NTA column washed with one column volume of Buffer D. The flow-through containing the protein lacking the tag was collected and concentrated by ultra-filtration (centricon 10 kDa CW-Sartorius) and further purified by size-exclusion chromatography on an ENrich™ SEC 650 column pre-equilibrated in buffer E (20 mM Tris-HCl pH7.4 and 0.2 M NaCl) for crystallization or buffer F (20 mM Tris-HCl pH8 and 0.2 M NaCl) for kinetics measurements. The purity of the protein was estimated by Coomassie-blue stained SDS-PAGE.

For SeMet incorporation, the same expression plasmid was transformed into *E. coli* B834 (DE3) methionine auxotroph strain (Novagen). Cells were firstly grown in 2 liters of LB medium containing 50 µg/mL KAN at 37°C under agitation at 180 rpm for 24 h. This starter culture was then pelleted, washed thrice and resuspended in pre-warmed medium A containing M9 medium, trace elements, 20% glucose, 1M $MgSO_4$, 1M $CaCl_2$, biotin, thiamine and 50 µg/mL KAN to a final OD_{600} = ~0.8. The culture was incubated at 37°C for 1.5 h prior to addition of a mix of 100 µg/mL D/L-SeMet and kept for further 30 min of incubation. Finally, 1 mM of IPTG was added to induce the protein expression for 16 h at 16°C. The purification protocol and crystallization conditions of the SeMet-labelled protein were identical to those used for the native protein, as described above. Protein concentration was determined using a Nanodrop 2000c spectrophotometer (Thermo Scientific) according to the extinction coefficient of *Mabs*_Eis2 (60975 $M^{-1}.cm^{-1}$).

Kinetics assay

For the kinetic assays, proteins were freshly purified, concentrated to 2.5 mg/mL and kept at 4°C. The reaction was monitored at 25°C every 5 sec in a quartz cuvette using a Nanodrop 2000c spectrophotometer (Thermo Scientific) by monitoring the production of TNB (2-thio-5-nitrobenzoic acid, extinction coefficient : 14150 $M^{-1}cm^{-1}$) at 412 nm for 90 s which is generated upon reduction of DTNB (5,5-dithio-bis-(nitrobenzoic acid) (Sigma-Aldrich) by the free CoA-SH released during the acetyltransferase reaction. All compounds, KAN (a mixture of kanamycin A (96%) and B (4%), Euromedex), HYG (Euromedex), AMK (Sigma-Aldrich) and enzyme were dissolved and diluted in buffer F. The enzyme (0.25 µM) was first incubated with a saturating concentration of acetyl-CoA (1 mM) (Sigma-Aldrich) for 2 min prior to initiating the reaction with DTNB (2 mM) and a range of antibiotic concentrations in a final volume of 80 µl. All absorbance values were normalized against a negative control where the antibiotic was absent and standard errors were calculated from three replicates. Nonlinear least-squares regression algorithm was used to determine the Michaelis-Menten equation (GraphPad Prism software).

Determination of molecular weight by size-exclusion chromatography

The oligomeric state of *Mabs*_Eis2 in solution was assessed on a Superdex 200 Increase 10/300 GL gel filtration column (GE healthcare) and eluted with buffer F described above at a flow rate of 0.4 mL/min at 4°C. The molecular weight was determined based on a calibration curve obtained using the Gel Filtration Markers Kit for protein molecular mass 12 400–200 000 Da (Sigma-Aldrich) and dextran blue to assess the column void volume. The apparent mass was obtained by plotting the partition coefficient K_{av} against the logarithms of the molecular weight of standard proteins.

Crystallization

The *apo*-form of the *Mabs*_Eis2 SeMet crystals were grown in sitting drops in MR Crystallization Plates™ (Hampton Research) at 18°C by mixing 2 µl of protein solution concentrated to 4 mg/mL with 2 µL of reservoir solution consisting of 0.2 M ammonium acetate, 0.1 M sodium citrate pH 5.5, 24% w/v PEG 4000 and 5 mM HYG. Crystals were cryoprotected by a brief soaking step into a solution of 0.2 M Ammonium acetate, 0.1 M sodium citrate pH 5.5, 30% w/v PEG 4000, 5 mM HYG and 10% PEG 400 prior to being cryo-cooled in liquid nitrogen.

The crystals of the native *Mabs*_Eis2 protein were obtained in sitting drops in 96-well SWISSCI MRC plates (Molecular Dimension) at 18°C by mixing 0.8 µl of protein solution at 12 mg/mL

with 0.8 µL of reservoir solution made of 0.2 M lithium sulfate monohydrate, 0.1 M BIS-TRIS pH 5.5, 25% w/v PEG 3350. Crystals were not cryo-protected prior to being stored in liquid nitrogen.

The acetyl-CoA bound form of *Mabs*_Eis2 crystals was obtained using the SeMet-labeled protein and were grown in sitting drops in MR Crystallization Plates™ (Hampton Research) at 18°C by mixing 2 µL of protein solution concentrated to 4 mg/mL with 2 µL of reservoir solution consisting of 0.1 M BIS-TRIS pH 5.5, 27% PEG 3350 and 2 mM acetyl-CoA. Crystals were briefly soaked into a solution containing 0.1 M BIS-TRIS pH 5.5, 30% PEG 3350, 2mM acetyl-CoA and 10% PEG 400 prior to being cryo-cooled in liquid nitrogen.

Data collection, structure determination, and refinement

All datasets were collected at the X06DA-PXIII beamline at the Swiss Light Source, Villigen, Switzerland. Data were processed, scaled and merged with *XDS* [37] and the high-resolution limit was determined according to the $CC_{1/2}$ values [38]. The *Mabs*_Eis2 structure was solved by the Single-wavelength Anomalous Dispersion method using *Autosol* from the *Phenix* package [39]. The two other structures were solved by molecular replacement performed with *Phaser* [40] from the *Phenix* package and using the *Mabs*_Eis2:ACO model as a search model. *Coot* [41] was used for manual rebuilding, while structure refinement and validation were performed with the *Phenix* package. The statistics for the data collection and structure refinement are displayed in Table 1. Figures were prepared with PyMOL (www.pymol.org).

***In silico* docking**

Aminoglycosides docking was performed with the *PyRx* software [42] running *AutoDock Vina* [43] and using the chain A of the *Mabs*_Eis2:ACO crystal structure as a receptor. HYG, KAN, and AMK were all docked with the following grid parameters center X=29.5 Y=7.2 Z=59.7 and dimensions (Å) X=25.9, Y=20.5, and Z=24.5. Residues 26, 117, 195, 228, 245, 274, 410 and 411 were defined as flexible

References

1 Ryan K & Byrd TF (2018) Mycobacterium abscessus: Shapeshifter of the Mycobacterial World. *Front. Microbiol.* **9**, 2642.

2 Griffith DE, Girard WM & Wallace RJ Jr (1993) Clinical features of pulmonary disease caused by rapidly growing mycobacteria. An analysis of 154 patients. *Am Rev Respir Dis* **147**, 1271–1278.

3 Roux A-L, Catherinot E, Ripoll F, Soismier N, Macheras E, Ravilly S, Bellis G, Vibet M-A, Le Roux E, Lemonnier L, Gutierrez C, Vincent V, Fauroux B, Rottman M, Guillemot D, Gaillard J-L & Jean-Louis Herrmann for the OMA Group (2009) Multicenter study of prevalence of nontuberculous mycobacteria in patients with cystic fibrosis in france. *J Clin Microbiol* **47**, 4124–4128.

4 Bryant JM, Grogono DM, Rodriguez-Rincon D, Everall I, Brown KP, Moreno P, Verma D, Hill E, Drijkoningen J, Gilligan P, Esther CR, Noone PG, Giddings O, Bell SC, Thomson R, Wainwright CE, Coulter C, Pandey S, Wood ME, Stockwell RE, Ramsay KA, Sherrard LJ, Kidd TJ, Jabbour N, Johnson GR, Knibbs LD, Morawska L, Sly PD, Jones A, Bilton D, Laurenson I, Ruddy M, Bourke S, Bowler ICJW, Chapman SJ, Clayton A, Cullen M, Dempsey O, Denton M, Desai M, Drew RJ, Edenborough F, Evans J, Folb J, Daniels T, Humphrey H, Isalska B, Jensen-Fangel S, Jönsson B, Jones AM, Katzenstein TL, Lillebaek T, MacGregor G, Mayell S, Millar M, Modha D, Nash EF, O'Brien C, O'Brien D, Ohri C, Pao CS, Peckham D, Perrin F, Perry A, Pressler T, Prtak L, Qvist T, Robb A, Rodgers H, Schaffer K, Shafi N, van Ingen J, Walshaw M, Watson D, West N, Whitehouse J, Haworth CS, Harris SR, Ordway D, Parkhill J & Floto RA (2016) Emergence and spread of a human-transmissible multidrug-resistant nontuberculous mycobacterium. *Science* **354**, 751–757.

5 Strnad L & Winthrop KL (2018) Treatment of Mycobacterium abscessus Complex. *Semin. Respir. Crit. Care Med.* **39**, 362–376.

6 Nessar R, Cambau E, Reyrat JM, Murray A & Gicquel B (2012) Mycobacterium abscessus: a new antibiotic nightmare. *J Antimicrob Chemother* **67**, 810–818.

7 Jarlier V & Nikaido H (1994) Mycobacterial cell wall: structure and role in natural resistance to antibiotics. *FEMS Microbiol Lett* **123**, 11–18.

8 Nash KA, Brown-Elliott BA & Wallace RJ Jr (2009) A novel gene, erm(41), confers inducible macrolide resistance to clinical isolates of Mycobacterium abscessus but is absent from Mycobacterium chelonae. *Antimicrob Agents Chemother* **53**, 1367–1376.

9 Prammananan T, Sander P, Brown BA, Frischkorn K, Onyi GO, Zhang Y, Böttger EC & Wallace RJ Jr (1998) A single 16S ribosomal RNA substitution is responsible for resistance to amikacin and other 2-deoxystreptamine aminoglycosides in Mycobacterium abscessus and Mycobacterium chelonae. *J Infect Dis* **177**, 1573–1581.

10 Viljoen A, Dubois V, Girard-Misguich F, Blaise M, Herrmann J-L & Kremer L (2017) The diverse family of MmpL transporters in mycobacteria: from regulation to antimicrobial developments. *Mol. Microbiol.* **104**, 889–904.

11 Richard M, Gutiérrez AV, Viljoen AJ, Ghigo E, Blaise M & Kremer L (2018) Mechanistic and Structural Insights Into the Unique TetR-Dependent Regulation of a Drug Efflux Pump in Mycobacterium abscessus. *Front. Microbiol.* **9**, 649.

12 Richard M, Gutiérrez AV, Viljoen A, Rodriguez-Rincon D, Roquet-Baneres F, Blaise M, Everall I, Parkhill J, Floto RA & Kremer L (2019) Mutations in the MAB_2299c TetR Regulator Confer Cross-Resistance to Clofazimine and Bedaquiline in Mycobacterium abscessus. *Antimicrob. Agents Chemother.* **63**, e01316-18.

13 Hohl M, Remm S, Eskandarian HA, Molin MD, Arnold FM, Hürlimann LM, Krügel A, Fantner GE, Sander P & Seeger MA (2019) Increased drug permeability of a stiffened mycobacterial outer membrane in cells lacking MFS transporter Rv1410 and lipoprotein LprG. *Mol. Microbiol.* **111**, 1263–1282.

14 Luthra S, Rominski A & Sander P (2018) The Role of Antibiotic-Target-Modifying and Antibiotic-Modifying Enzymes in Mycobacterium abscessus Drug Resistance. *Front. Microbiol.* **9**, 2179.

15 Dubée V, Bernut A, Cortes M, Lesne T, Dorchene D, Lefebvre A-L, Hugonnet J-E, Gutmann L, Mainardi J-L, Herrmann J-L, Gaillard J-L, Kremer L & Arthur M (2015) β-Lactamase inhibition by avibactam in Mycobacterium abscessus. *J Antimicrob Chemother* **70**, 1051–1058.

16 Lefebvre A-L, Moigne VL, Bernut A, Veckerlé C, Compain F, Herrmann J-L, Kremer L, Arthur M & Mainardi J-L (2017) Inhibition of the β-Lactamase BlaMab by Avibactam Improves the In Vitro and In Vivo Efficacy of Imipenem against Mycobacterium abscessus. *Antimicrob. Agents Chemother.* **61**, e02440-16.

17 Dal Molin MD, Gut M, Rominski A, Haldimann K, Becker K & Sander P (2018) Molecular Mechanisms of Intrinsic Streptomycin Resistance in Mycobacterium abscessus. *Antimicrob. Agents Chemother.* **62**, e01427-17.

18 Rominski A, Selchow P, Becker K, Brülle JK, Dal Molin M & Sander P (2017) Elucidation of Mycobacterium abscessus aminoglycoside and capreomycin resistance by targeted deletion of three putative resistance genes. *J. Antimicrob. Chemother.* **72**, 2191–2200.

19 Wei J, Dahl JL, Moulder JW, Roberts EA, O'Gaora P, Young DB & Friedman RL (2000) Identification of a Mycobacterium tuberculosis gene that enhances mycobacterial survival in macrophages. *J. Bacteriol.* **182**, 377–384.

20 Samuel LP, Song C-H, Wei J, Roberts EA, Dahl JL, Barry CE, Jo E-K & Friedman RL (2007) Expression, production and release of the Eis protein by Mycobacterium tuberculosis during infection of macrophages and its effect on cytokine secretion. *Microbiol. Read. Engl.* **153**, 529–540.

21 Duan L, Yi M, Chen J, Li S & Chen W (2016) Mycobacterium tuberculosis EIS gene inhibits macrophage autophagy through up-regulation of IL-10 by increasing the acetylation of histone H3. *Biochem. Biophys. Res. Commun.* **473**, 1229–1234.

22 Shin D-M, Jeon B-Y, Lee H-M, Jin HS, Yuk J-M, Song C-H, Lee S-H, Lee Z-W, Cho S-N, Kim J-M, Friedman RL & Jo E-K (2010) Mycobacterium tuberculosis eis regulates autophagy, inflammation, and cell death through redox-dependent signaling. *PLoS Pathog.* **6**, e1001230.

23 Ghosh S, Padmanabhan B, Anand C & Nagaraja V (2016) Lysine acetylation of the Mycobacterium tuberculosis HU protein modulates its DNA binding and genome organization. *Mol. Microbiol.* **100**, 577–588.

24 Kim KH, An DR, Song J, Yoon JY, Kim HS, Yoon HJ, Im HN, Kim J, Kim DJ, Lee SJ, Kim K-H, Lee H-M, Kim H-J, Jo E-K, Lee JY & Suh SW (2012) Mycobacterium tuberculosis Eis protein initiates suppression of host immune responses by acetylation of DUSP16/MKP-7. *Proc. Natl. Acad. Sci. U. S. A.* **109**, 7729–7734.

25 Zaunbrecher MA, Sikes RD, Metchock B, Shinnick TM & Posey JE (2009) Overexpression of the chromosomally encoded aminoglycoside acetyltransferase eis confers kanamycin resistance in Mycobacterium tuberculosis. *Proc. Natl. Acad. Sci. U. S. A.* **106**, 20004–20009.

26 Chen W, Biswas T, Porter VR, Tsodikov OV & Garneau-Tsodikova S (2011) Unusual regioversatility of acetyltransferase Eis, a cause of drug resistance in XDR-TB. *Proc. Natl. Acad. Sci. U. S. A.* **108**, 9804–9808.

27 Sanz-García F, Anoz-Carbonell E, Pérez-Herrán E, Martín C, Lucía A, Rodrigues L & Aínsa JA (2019) Mycobacterial Aminoglycoside Acetyltransferases: A Little of Drug Resistance, and a Lot of Other Roles. *Front. Microbiol.* **10**, 46.

28 Green KD, Pricer RE, Stewart MN & Garneau-Tsodikova S (2015) Comparative Study of Eis-like Enzymes from Pathogenic and Nonpathogenic Bacteria. *ACS Infect. Dis.* **1**, 272–283.

29 Dubois V, Pawlik A, Bories A, Moigne VL, Sismeiro O, Legendre R, Varet H, Rodriguez P, Gaillard J-L, Copee J-Y, Brosch R, Herrmann J-L & Girard-misguich F (2019) Mycobacterium abscessus virulence traits unraveled by transcriptomic profiling in amoeba and macrophages. *bioRxiv*, 529057.

30 Hurst-Hess K, Rudra P & Ghosh P (2017) Mycobacterium abscessus WhiB7 Regulates a Species-Specific Repertoire of Genes To Confer Extreme Antibiotic Resistance. *Antimicrob. Agents Chemother.* **61**, e01347-17.

31 Green KD, Biswas T, Chang C, Wu R, Chen W, Janes BK, Chalupska D, Gornicki P, Hanna PC, Tsodikov OV, Joachimiak A & Garneau-Tsodikova S (2015) Biochemical and structural analysis of an Eis family aminoglycoside acetyltransferase from bacillus anthracis. *Biochemistry* **54**, 3197–3206.

32 Krissinel E & Henrick K (2007) Inference of macromolecular assemblies from crystalline state. *J. Mol. Biol.* **372**, 774–797.

33 Svergun DI, Barberato C & Koch MHJ (1995) CRYSOL - a Program to Evaluate X-ray Solution Scattering of Biological Macromolecules from Atomic Coordinates. *J Appl Cryst* **28**, 768–773.

34 Kim KH, An DR, Yoon HJ, Yang JK & Suh SW (2014) Structure of Mycobacterium smegmatis Eis in complex with paromomycin. *Acta Crystallogr. Sect. F Struct. Biol. Commun.* **70**, 1173–1179.

35 Houghton JL, Biswas T, Chen W, Tsodikov OV & Garneau-Tsodikova S (2013) Chemical and structural insights into the regioversatility of the aminoglycoside acetyltransferase Eis. *Chembiochem Eur. J. Chem. Biol.* **14**, 2127–2135.

36 Novosad SA, Beekmann SE, Polgreen PM, Mackey K, Winthrop KL & M. abscessus Study Team (2016) Treatment of Mycobacterium abscessus Infection. *Emerg. Infect. Dis.* **22**, 511–514.

37 Kabsch W (2010) Integration, scaling, space-group assignment and post-refinement. *Acta Crystallogr. D Biol. Crystallogr.* **66**, 133–144.

38 Karplus PA & Diederichs K (2012) Linking crystallographic model and data quality. *Science* **336**, 1030–1033.

39 Adams PD, Afonine PV, Bunkóczi G, Chen VB, Davis IW, Echols N, Headd JJ, Hung L-W, Kapral GJ, Grosse-Kunstleve RW, McCoy AJ, Moriarty NW, Oeffner R, Read RJ, Richardson DC, Richardson JS, Terwilliger TC & Zwart PH (2010) PHENIX: a comprehensive Python-based system for macromolecular structure solution. *Acta Crystallogr. D Biol. Crystallogr.* **66**, 213–221.

40 McCoy AJ, Grosse-Kunstleve RW, Adams PD, Winn MD, Storoni LC & Read RJ (2007) Phaser crystallographic software. *J. Appl. Crystallogr.* **40**, 658–674.

41 Emsley P, Lohkamp B, Scott WG & Cowtan K (2010) Features and development of Coot. *Acta Crystallogr. D Biol. Crystallogr.* **66**, 486–501.

42 Dallakyan S & Olson AJ (2015) Small-molecule library screening by docking with PyRx. *Methods Mol Biol* **1263**, 243–250.

43 Trott O & Olson AJ (2010) AutoDock Vina: improving the speed and accuracy of docking with a new scoring function, efficient optimization, and multithreading. *J. Comput. Chem.* **31**, 455–461.

44 Robert X & Gouet P (2014) Deciphering key features in protein structures with the new ENDscript server. *Nucleic Acids Res* **42**, W320–324.

Table 1 Data collection and Refinement statistics

Data collection statistics	Eis2_apo_form	Eis2_apo_form_SeMet	Eis2_ACO
Beamline	X06DA-PXIII	X06DA-PXIII	X06DA-PXIII
Wavelength (Å)	0.99	0.979	0.979
Resolution range (Å)	46.4 - 2.2 (2.27 - 2.2)	49.6 - 1.9 (1.96 - 1.9)	48.9 - 2.3 (2.38 - 2.3)
Space group	P 1 21 1	P 1 21 1	P 1 21 1
Unit cell (Å,°)	112.6 79.8 152.8 90 90.2 90	112.4 79.8 152.6 90 90.2 90	111.6 76.9 152.5 90 90.8 90
Total reflections	919521 (94036)	1452488 (145654)	785863 (79328)
Multiplicity	6.7 (6.8)	6.8 (6.9)	6.8 (6.9)
Completeness (%)	99.9 (99.6)	98.9 (90.5)	99.9 (99.9)
Mean I/sigma(I)	12.2 (1.4)	11.8 (1.1)	8.9 (1.8)
Wilson B-factor ($Å^2$)	42.5	30.0	30.3
R-meas	0.141 (1.61)	0.133 (1.81)	0.228 (1.16)

CC1/2	0.99 (0.60)	0.99 (0.51)	0.99 (0.53)
CC*	1 (0.86)	1 (0.82)	0.99 (0.83)
Data refinement statistics			
Reflections used in refinement	137956 (13688)	210833 (19143)	115358 (11494)
R-work	0.199 (0.387)	0.201 (0.403)	0.229 (0.298)
R-free	0.230 (0.415)	0.226 (0.431)	0.266 (0.337)
Number of non-H atoms	19964	20624	20077
macromolecules	18878	18820	18824
ligands	100	190	285
solvent	986	1614	968
Protein residues	2431	2424	2425
RMS bonds (Å)	0.002	0.003	0.002
RMS angles (°)	0.55	0.57	0.48
Ramachandran favored (%)	98.59	97.99	97.88

Ramachandran allowed (%)	1.41	2.01	2.12
Ramachandran outliers(%)	0	0	0
Rotamer outliers (%)	0.61	0.96	0.66
Average B-factor (Å^2)	54.7	43.9	41.9
macromolecules	54.9	43.8	41.8
ligands	79.6	58.4	68.9
solvent	49.0	43.6	35.4
Clashscore	2.53	2.18	4.16
PDB accession number	6RFY	6RFX	6RFT

Table 2: Kinetic parameters of *Mabs*_Eis2

	V_{max} (µM.s^{-1})	K_M (µM)	k_{cat} (s^{-1})	k_{cat}/K_M (M^{-1} s^{-1})
Kanamycin	0.49 ± 0.074	504.67 ± 222.89	1.96 ± 0.29	4.27 x 10^3 ± 1.3 x 10^3
Hygromycin B	0.98 ± 0.14	66.15 ± 25.67	3.93 ± 0.57	6.29 x 10^4 ± 14.2 x 10^4
Amikacin	0.67 ± 0.062	59.55 ± 6.5	2.68 ± 0.25	4.51 x 10^4 ± 4.27 x 10^3

Acknowledgments

We thank the staff at SLS beamlines for support during data collection. KLU Ph.D. fellowship is supported by the National Research Agency [ANR-17-CE11-0008-01 – MyTraM to MB], the Fondation pour la Recherche Médicale (FRM) [grant number DEQ20150331719 to LK]. HMAB is supported by a fellowship from the Lunbeck Foundation. The research leading to these results has received funding from the European Community's Horizon 2020 Framework Programme under grant agreement nº 730872.

Author contributions

MB designed the study. KLU, HMAB, and MB performed biochemical and crystallization experiments. KLU, VO, and MB collected the x-ray data. KLU determined the kinetic constants. MB solved and refined the crystal structures. LK and MB supervised the project. MB wrote the first draft and all the authors contributed to the proofreading of the manuscript.

Conflicts of interest

The authors declare no conflict of interest.

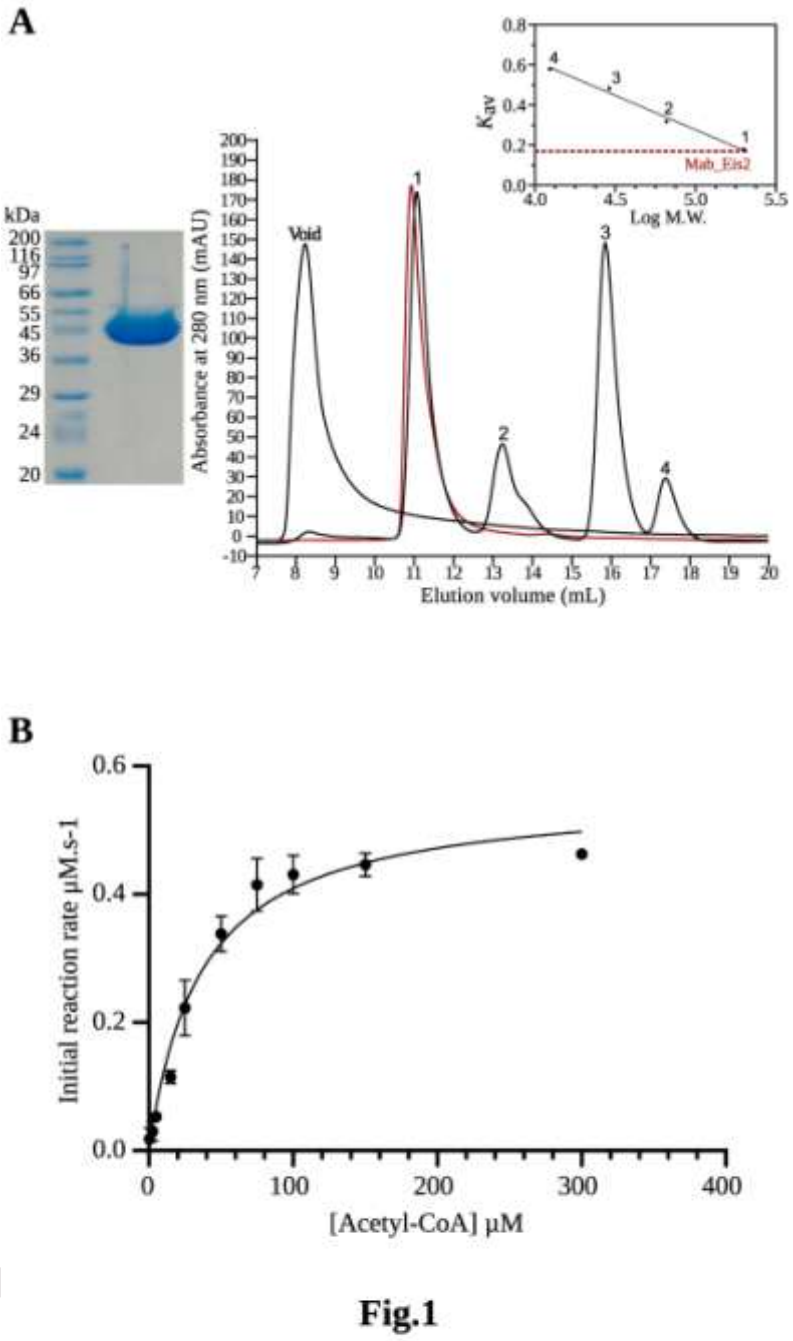

Fig.1

Figure 1: Biochemical characterization of *Mabs*_Eis2

A Coomassie Blue-stained SDS polyacrylamide gel electrophoresis of *Mabs*_Eis2 obtained after three steps of purification (10 µg of protein were loaded on the gel). Estimation of the oligomeric state of *Mabs*_Eis2 depleted from its tags by size-exclusion chromatography. The elution profile of the proteins used for calibration is displayed as a black line and the elution profile of *Mabs*_Eis2 is shown in red. Calibration was established using β-amylase (1) (200 kDa), bovine serum albumin (2) (66 kDa), carbonic anhydrase (3) (29 kDa), and cytochrome C (4) (12.4 kDa), eluted with estimated volumes of 11.06, 13.23, 15.85 and 17.38 mL, respectively. The void volume was estimated at 8.23 mL with dextran blue. The *Mabs*_Eis2 elution peak at 10.91 mL corresponds to an apparent molecular weight of 205 kDa. **B** Michaelis and Menten curve used to determine the kinetic constants for acetyl-CoA in presence of KAN.

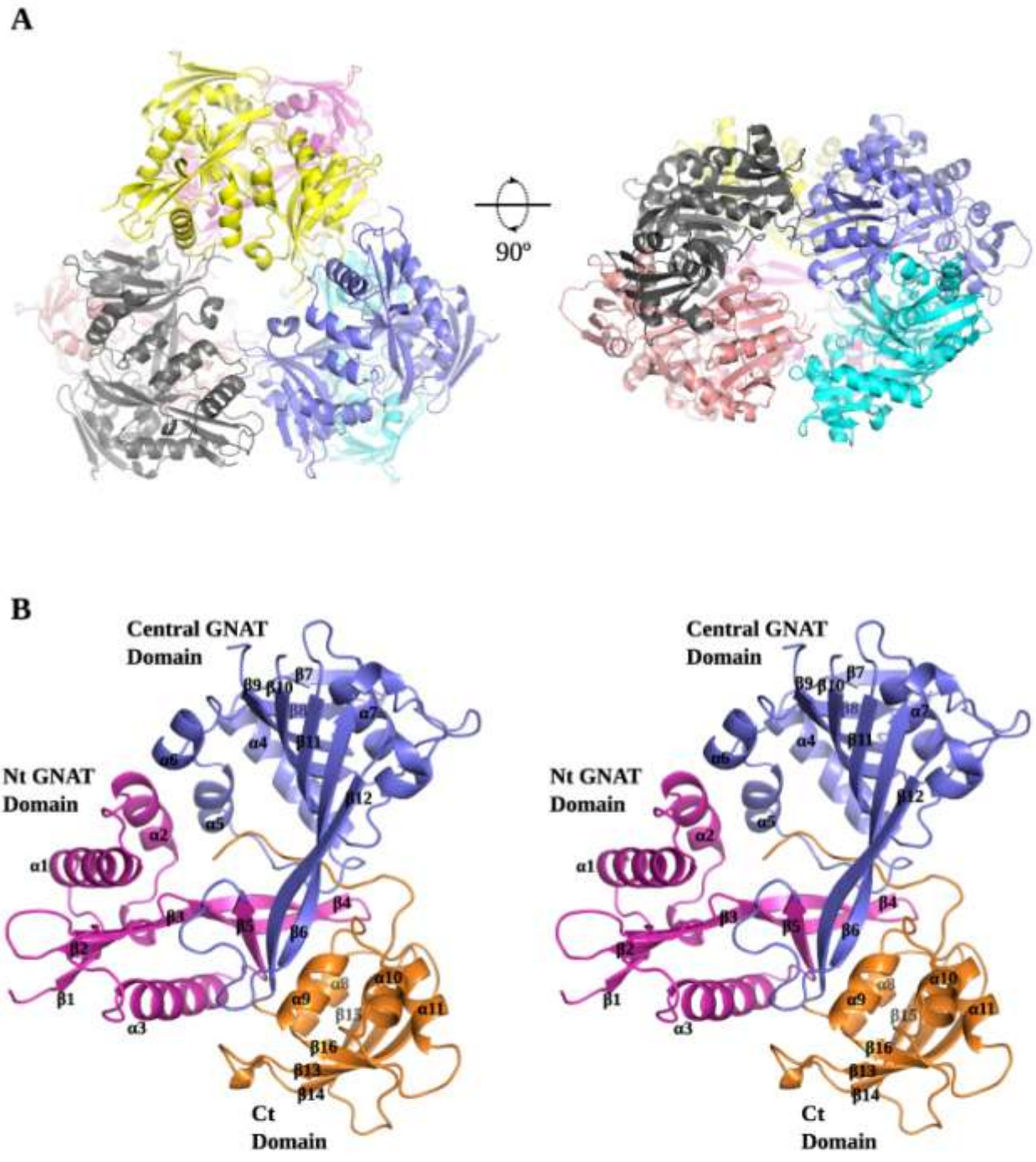

Fig.2

Figure 2: Overall structure of the *Mabs*_Eis2 *apo*-form

A The figure displays the asymmetric unit composition reflecting the biological oligomeric state of *Mabs*_Eis2. **B** Stereo-view of the monomeric form of *Mabs*_Eis2. The protein can be divided into three domains the N-terminal (Nt) domain GNAT colored in magenta, the central GNAT domain in blue slate and the C-terminal (Ct) domain in orange. The α and β signs followed by numbers indicate respectively the alpha-helices and beta-strands numbering.

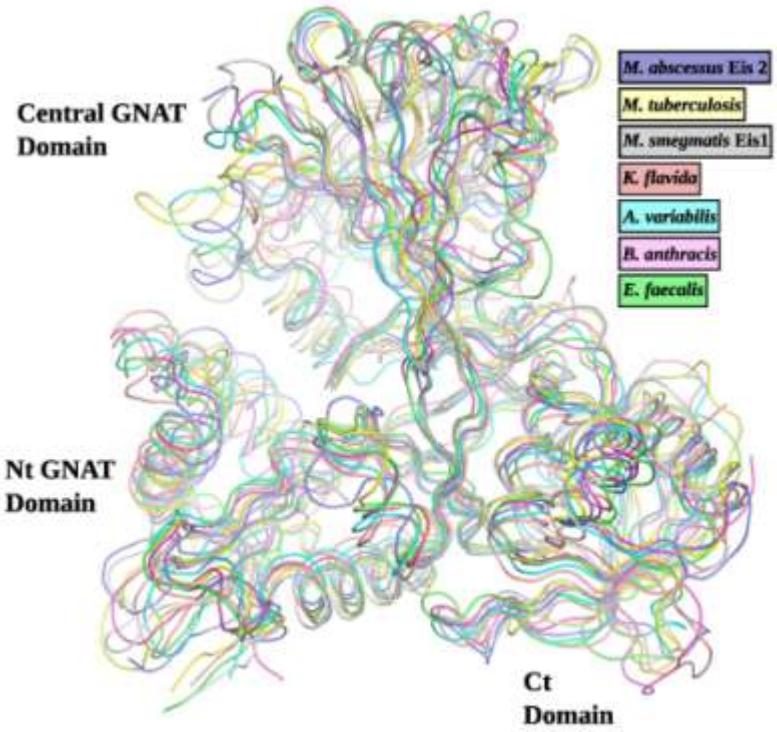

Fig.3

Figure 3: Structural comparison of Eis protein structures.

Superposition of all the bacterial Eis protein structures retrieved from the protein data bank onto *Mabs*_Eis2. The different proteins are in ribbon representation and with the following colors: *M. abscessus* Eis2 in slate blue, *M. tuberculosis* (PDB : 3uy5) in yellow, *M. smegmatis* (PDB : 4qb9) in grey, *Bacillus anthracis* (PDB : 3n7z) in magenta, *Enterococcus faecalis* (PDB : 2hv2) in green, *Anabaena variabilis* (PDB : 2ozg) in cyan blue and *Kribbella flavida* (PDB : 4my3) in salmon. The different domains are indicated, Nt and Ct stand for for N- and C-terminus respectively.

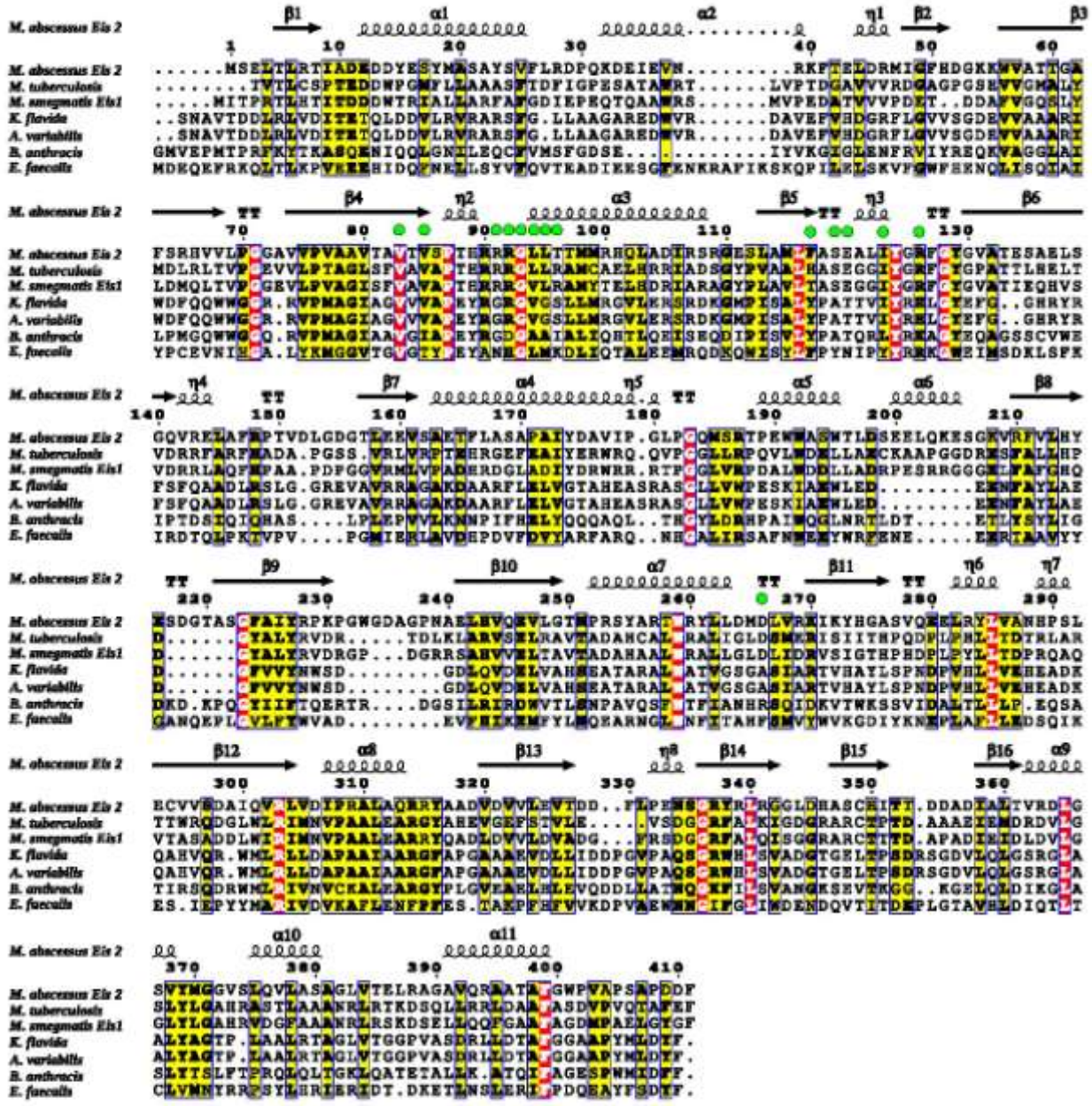

Fig.4

Figure 4: Multiple sequence alignment of Eis and Eis-like proteins

The multiple sequence alignment was performed with ClustalX and the display was made using the ESPript 3 server [44]. The secondary structure (α, α-helix; β, β-strand, TT, β-turn; η, 3 10 -helix) of *Mabs*_Eis2 extracted from its crystal structure, is indicated on top of the alignment. Residues involved in ACO binding in *Mabs*_Eis2 are indicated by the green circles.

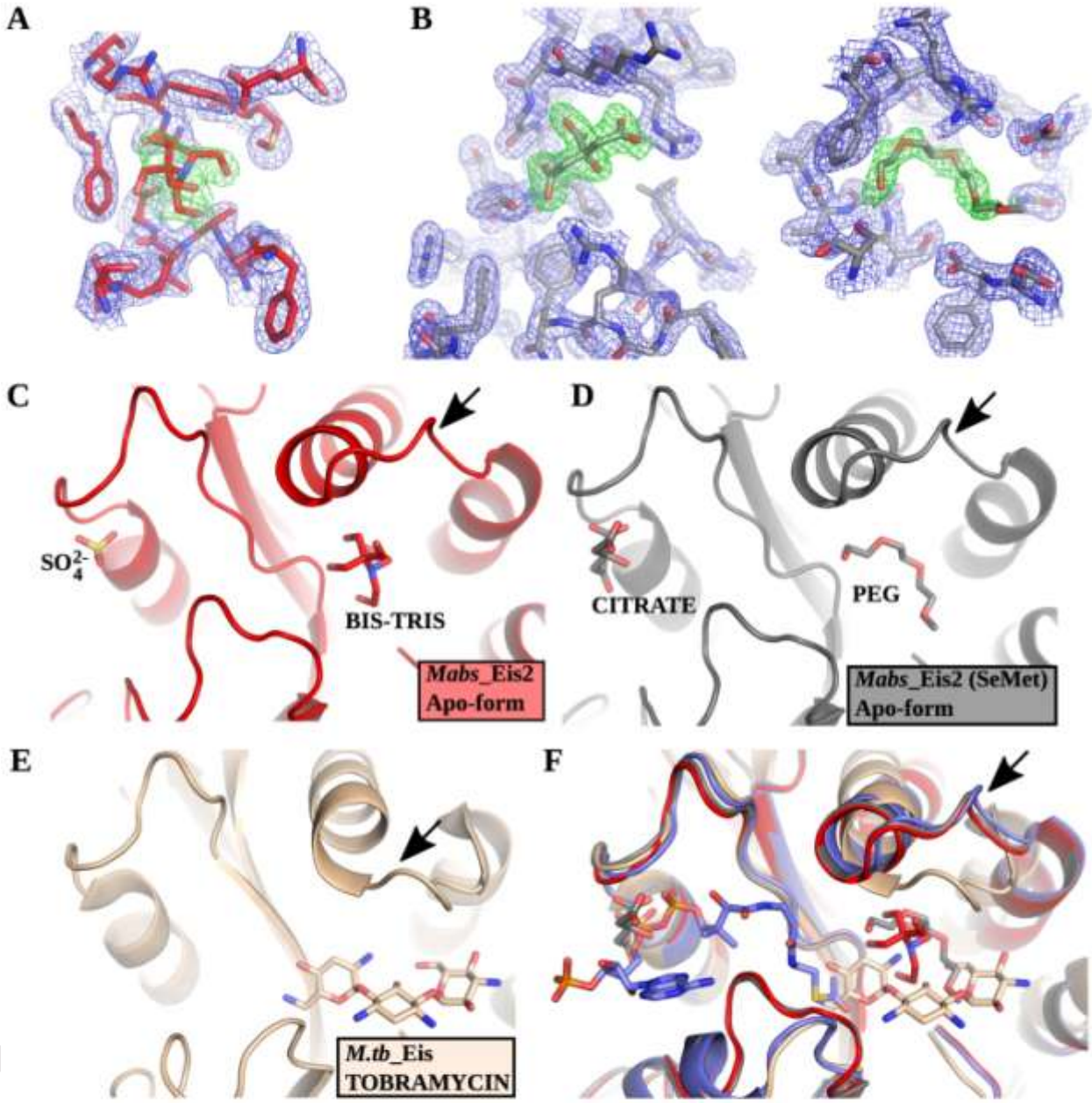

Fig.5

Figure 5: Binding of ligands found in the crystallization conditions

All the structures are shown in cartoon representation. **A** and **B** represent the 2Fo-Fc electron density map, shown as a blue mesh and contoured at 1 σ level for the residues surrounding the ligands : BIS-TRIS, citrate and PEG, as seen in the two crystal structures of the *apo*-form. The simulated annealed Fo-Fc omit map for each ligand is contoured at 2.8 σ level and shown in green mesh. **C** shows the *apo*-form structure (in red) bound to a BIS-TRIS molecule, **D** represents the *apo*-form structure (in grey) obtained with the SeMet-labeled protein bound to a citrate and PEG molecules. E displays the *M. tuberculosis* Eis crystal structure (wheat color) bound to ACO (not shown) and tobramycin (PDB: 4jd6). The superposition of all the structures is depicted in F and shows that the SO_4^{2-} ion or citrate occupy the ACO binding site as in the *Mabs*_Eis2 structure bound to ACO (in blue) and that BIS-TRIS or PEG share the same cavity than tobramycin. The black arrows point the loop region moving upon AG binding in the *M. tuberculosis* Eis crystal structure, the same region in the *Mabs*_Eis2 structure is not affected upon binding of PEG or BIS-TRIS.

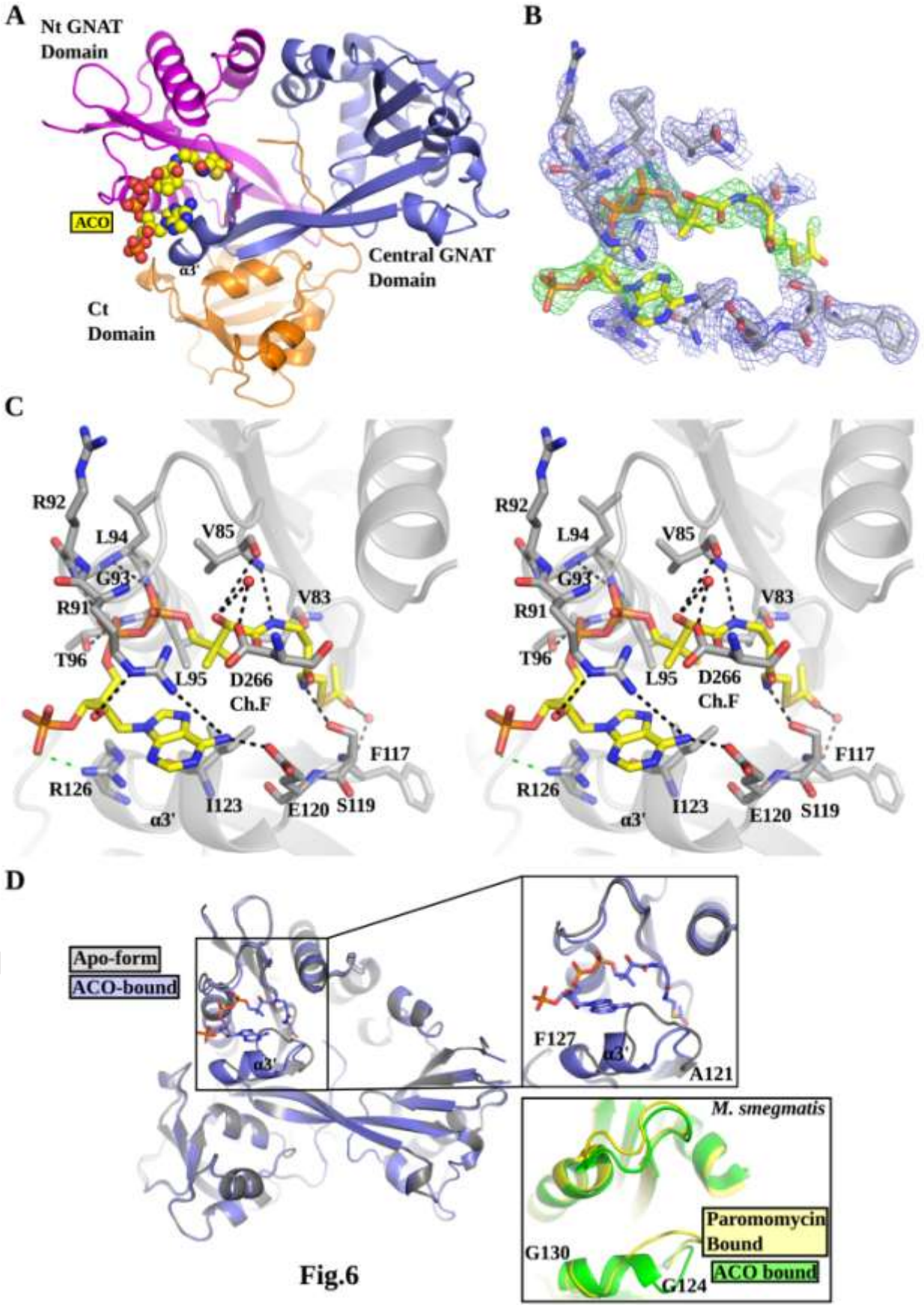

Fig.6

Figure 6: Crystal structure of *Mabs*_Eis2 bound to acetyl-CoA

A The overall structure of the monomer of *Mabs*_Eis2 bound to ACO **is** shown in cartoon representation. The cofactor (ACO) shown as yellow sticks is binding between the Nt and central GNAT domains. The helix appearing after ACO binding was named α3'. **B** The panel displays the $2F_o$-F_c electron density map in blue and contoured at 1 σ level of the modelled residues in the vicinity of ACO. The simulated annealed F_o-F_c OMIT map contoured at 2.8 σ level and displayed as a green mesh and as seen in chain A attests to the presence of ACO in the crystal structure. **C** Stereo-view of the ACO (in yellow) binding site. H-bonds are indicated by the black dashed lines while the salt-bridge is marked with the dashed green line. Water molecules are represented by the red spheres. **D** Superimposition of the *apo*-form in grey onto the ACO bound form of *Mabs*_Eis2 (blue slate). The figure illustrates the structural rearrangement of residues Ala121 to Phe127 (helix α3') upon ACO recognition, a similar conformational change was observed in the *M. smegmatis* Eis structure (Gly124 to Gly130). The paromomycin bound form (PDB : 4qb9) is in yellow and ACO-bound complex is in green (PDB : 3sxn).

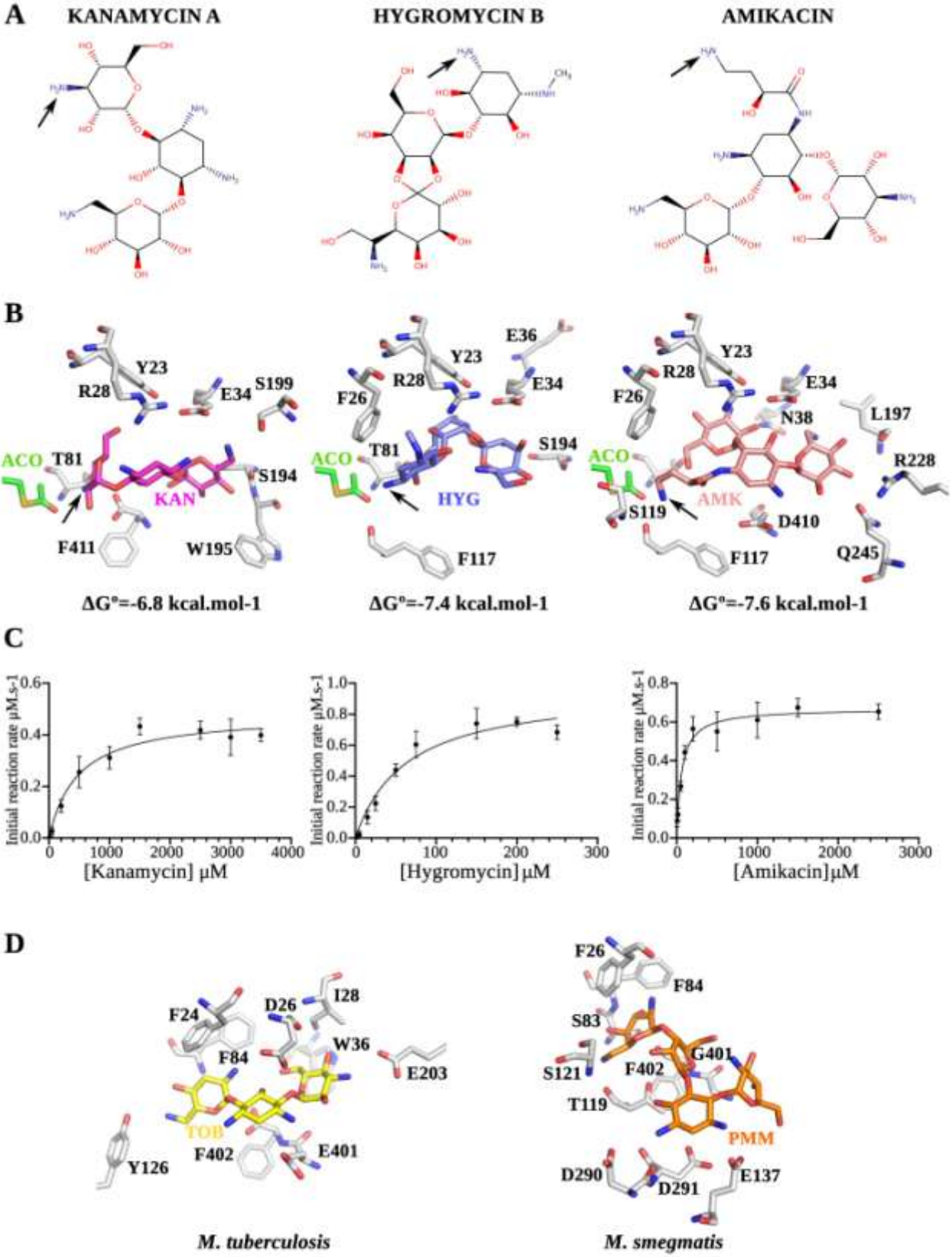

Fig.7

Figure 7: Aminoglycosides recognition

A Chemical structures of kanamycin A, hygromycin B, and amikacin. **B** Docking poses of the three different AG and mapping of the potential interacting amino acids. The scoring indicated by the ΔG values predicts similar binding energies for the three antibiotics. The black arrows indicate the position that can be acetylated in the proximity of the acetyl group of ACO shown in green sticks. **C** Michaelis and Menten curves used to determine the kinetic constants for the three AG. Kanamycin corresponds to a mixture of kanamycin A (96%) and B (4%). **D** Binding sites of tobramycin and paromomycin as seen in the co-crystal structures of Eis bound to AG from *M. tuberculosis* (PDB: 4jd6) and *M. smegmatis* (PDB: 4qb9).